

## Observation of an Incommensurate Charge Density Wave in Monolayer $\text{TiSe}_2/\text{CuSe}/\text{Cu}(111)$ Heterostructure


Zhipeng Song<sup>1</sup>, Jierui Huang<sup>1</sup>, Shuai Zhang<sup>1</sup>, Yun Cao<sup>1</sup>, Chen Liu<sup>2</sup>, Ruizi Zhang<sup>1</sup>, Qi Zheng<sup>1</sup>, Lu Cao<sup>1</sup>, Li Huang<sup>1</sup>, Jiaou Wang<sup>2</sup>, Tian Qian<sup>1,3,4</sup>, Hong Ding<sup>1,3,4</sup>, Wu Zhou<sup>1,4</sup>, Yu-Yang Zhang<sup>1,4</sup>, Hongliang Lu<sup>1,4,\*</sup>, Chengmin Shen<sup>1,4</sup>, Xiao Lin<sup>1,4,†</sup>, Shixuan Du<sup>1,3,4</sup> and Hong-Jun Gao<sup>1,3,4</sup>

<sup>1</sup>*Institute of Physics and University of Chinese Academy of Sciences, Chinese Academy of Sciences, Beijing 100190, China*

<sup>2</sup>*Institute of High Energy Physics, Chinese Academy of Sciences, Beijing 100049, China*

<sup>3</sup>*Songshan Lake Materials Laboratory, Dongguan, Guangdong 523808, China*

<sup>4</sup>*CAS Center for Excellence in Topological Quantum Computation, University of Chinese Academy of Sciences, Beijing 100190, China*

 (Received 7 February 2021; revised 18 October 2021; accepted 14 December 2021; published 10 January 2022)

$\text{TiSe}_2$  is a layered material exhibiting a commensurate ( $2 \times 2 \times 2$ ) charge density wave (CDW) with a transition temperature of  $\sim 200$  K. Recently, incommensurate CDW in bulk  $\text{TiSe}_2$  draws great interest due to its close relationship with the emergence of superconductivity. Here, we report an incommensurate superstructure in monolayer  $\text{TiSe}_2/\text{CuSe}/\text{Cu}(111)$  heterostructure. Characterizations by low-energy electron diffraction and scanning tunneling microscopy show that the main wave vector of the superstructure is  $\sim 0.41a^*$  or  $\sim 0.59a^*$  (here  $a^*$  is in-plane reciprocal lattice constant of  $\text{TiSe}_2$ ). After ruling out the possibility of moiré superlattices, according to the correlation of the wave vectors of the superstructure and the large indirect band gap below the Fermi level, we propose that the incommensurate superstructure is associated with an incommensurate charge density wave (I-CDW). It is noteworthy that the I-CDW is robust with a transition temperature over 600 K, much higher than that of commensurate CDW in pristine  $\text{TiSe}_2$ . Based on our data and analysis, we present that interface effect may play a key role in the formation of the I-CDW state.

DOI: [10.1103/PhysRevLett.128.026401](https://doi.org/10.1103/PhysRevLett.128.026401)

Transition metal dichalcogenides (TMDs) show a number of interesting properties, and one of them is CDW, which is still not fully understood [1,2].  $\text{TiSe}_2$  is one of the most studied CDW materials due to its simple commensurate ( $2 \times 2 \times 2$ ) CDW superstructure below  $T_{\text{CDW}} \approx 200$  K in the bulk phase [3–9]. Early research suggested that the CDW originates from traditional Fermi-surface nesting [10]. However, parallel Fermi surface sheets have not been observed in TMDs [11]. The band-type Jahn-Teller mechanism is also proposed to explain the CDW transition in  $\text{TiSe}_2$  [12–15]. Recently, the excitonic condensate mechanism [4,16–23] has been proposed as yet another CDW scenario. However, those mechanisms are in dispute [13,15] and further in-depth study is still needed to understand how the CDW is formed in  $\text{TiSe}_2$ .

Modulated  $\text{TiSe}_2$  has also been found to exhibit transitions to different ground states below a critical temperature. With the intercalation of Cu, it becomes superconducting when the amount of intercalated Cu is close to  $x = 0.04$  in  $\text{Cu}_x\text{TiSe}_2$  [24]. Charge stripe domains form at Cu content of  $x < 0.02$  [25] while phase-shifted CDW domains form at a higher Cu content [25,26]. Similarly, the features of breaking up of the commensurate order are observed under intercalation of Ti atoms [27]. Another work shows a local real-space view of the achiral

$2 \times 2 \times 2$  CDW in  $\text{TiSe}_2$  with introduced interstitial Ti atoms [9]. Under high pressure, an incommensurate phase above the superconducting dome is observed [7]. By the application of a gate electric field, many-body states can be controlled in a  $\text{TiSe}_2$  thin film, and it was inferred that the emergence of superconductivity is correlated with incommensurate CDW states embedded in the commensurate CDW states [28]. Therefore, an incommensurate CDW state in  $\text{TiSe}_2$  is believed to play an important role in the emergence of superconductivity. Further study of the incommensurate CDW state should lead to a deeper understanding of collective quantum states in solids.

Here we modulate the properties of  $\text{TiSe}_2$  by the fabrication of a  $\text{TiSe}_2/\text{CuSe}$  heterostructure on a  $\text{Cu}(111)$  substrate. Low-energy electron diffraction (LEED) and scanning tunneling microscopy (STM) studies show a new incommensurate superstructure with a main wave vector of 0.41 or 0.59 times the in-plane reciprocal lattice constant of  $\text{TiSe}_2$ , which is distinctly different from previous reports about incommensurate CDW [26]. The superstructure exists in a wide temperature range and even above room temperature. The possibility of moiré superlattices was excluded by the formula of moiré pattern periodicity. Angular-resolved photoemission spectroscopy (ARPES) results exhibit strong electron doping and a large

indirect band gap in the  $\text{TiSe}_2$  layer. Therefore, we conclude that the superstructure is associated with incommensurate CDW and propose a possible mechanism to explain it.

Monolayer  $\text{TiSe}_2$  was grown on the  $\text{CuSe}/\text{Cu}(111)$  surface in an ultrahigh-vacuum molecular beam epitaxy (MBE) system with a base pressure better than  $3 \times 10^{-10}$  mbar. First, the  $\text{Cu}(111)$  substrate was treated by cycles of argon-ion sputtering and annealing until the sharp diffraction spots were shown in a LEED pattern and clean surface was observed in STM images. Then, high purity Se (99.99%) was deposited on  $\text{Cu}(111)$  at a substrate temperature of 673 K to form monolayer  $\text{CuSe}$ . Finally, high purity Ti (99.99%) was deposited and followed by Se on  $\text{CuSe}/\text{Cu}(111)$  at the same substrate temperature. By these processes, the  $\text{TiSe}_2$  film formed on the  $\text{CuSe}/\text{Cu}(111)$  surface as shown in the schematics in Fig. 1(a). All of the characterizations were done in different ultrahigh vacuum chambers by using *in situ* transfer

technique. ARPES measurements were performed at a base pressure of  $\sim 6 \times 10^{-11}$  mbar and the photon energy was 40.8 eV. The energy resolution is less than 30 meV and the angular resolution is  $0.3^\circ$ .

STM topography in Fig. 1(b) shows two layers with different morphologies. The bottom layer [left part in Fig. 1(b)], with identical nanopores, is monolayer  $\text{CuSe}$  [29]. The top layer [right part in Fig. 1(b)] has a flat surface. Figure 1(c) is the atomic resolution STM image of this flat top layer, which has a hexagonal lattice with an interatomic spacing of 3.37 Å, in agreement with the top Se layer in  $\text{TiSe}_2$  [8,30]. X-ray photoelectron spectroscopy (XPS) measurement was performed to study the chemical compositions of the sample [see Figs. 1(d) and 1(e)]. The XPS peaks located at 461.2 and 455.1 eV in Fig. 1(d) can be attributed to  $\text{Ti } 2p_{1/2}$  and  $2p_{3/2}$  in  $\text{TiSe}_2$  [31]. The peaks at 54.8 and 54.0 eV in Fig. 1(e) are consistent with  $\text{Se } 3d_{3/2}$  and  $3d_{5/2}$  core levels in monolayer  $\text{CuSe}$  on  $\text{Cu}(111)$  [29], while those located at 54.4 and 53.6 eV are from  $\text{Se } 3d_{3/2}$  and  $3d_{5/2}$  in  $\text{TiSe}_2$ , respectively [31]. Combining STM and XPS characterizations, we confirm the formation of monolayer  $\text{TiSe}_2/\text{CuSe}$  heterostructure.

To investigate CDW properties in the as-fabricated heterostructure, we use STM to do further study at different temperatures. Figure 2(a) is the STM image of the top  $\text{TiSe}_2$  layer at 4.5 K, showing multiperiod atomic arrangement, indicating that it is a modulated  $\text{TiSe}_2$  ( $M\text{-TiSe}_2$ ). The FFT of Fig. 2(a) shown in Fig. 2(b) exhibits the reciprocal space of the  $\text{TiSe}_2$  lattice and superstructure clearly. Figure 2(c) is a representative line profile along the white line from the central point to  $M\text{-TiSe}_2$  point in Fig. 2(b). The peak positions indicate the periods of the superstructure of the sample. If we define the reciprocal lattice constant of  $M\text{-TiSe}_2$  as  $a^*$ , the reciprocal lattice constants of the superstructure is  $0.18a^*$  (peak 1),  $0.41a^*$  (peak 2), and  $0.59a^*$  (peak 3), indicating incommensurate superstructure in the STM image. We noticed that peak 3 is the strongest of the three peaks. The superstructure is very unique compared to previous reports, including commensurate ( $2 \times 2 \times 2$ ) superstructure in bulk  $1\text{T-TiSe}_2$  below 200 K [3] and incommensurate superstructure in  $\text{Cu}$ -intercalated bulk  $1\text{T-TiSe}_2$  at low temperature [26], which are associated to CDW.

The STM image at 80 K [Fig. 2(d)] is slightly different from that at 4.5 K. The FFT of Fig. 2(d) [Fig. 2(e)] shows nearly the same patterns of the superstructure as those at 4.5 K [Fig. 2(f)]. The superstructure still exists at room temperature based on the STM image shown in Fig. 2(g). However, one set of patterns disappear in the FFT shown in Fig. 2(h). Figure 2(i) is the line profile from the central point to  $M\text{-TiSe}_2$  point in Fig. 2(h). From Fig. 2(i) we find that peak 1 disappeared, while peak 2 still exists and peak 3 is weakened at room temperature. Peak 2 is the strongest peak. The positions of these peaks, determined from FFT of STM image at room temperature [Fig. 2(h)], are consistent

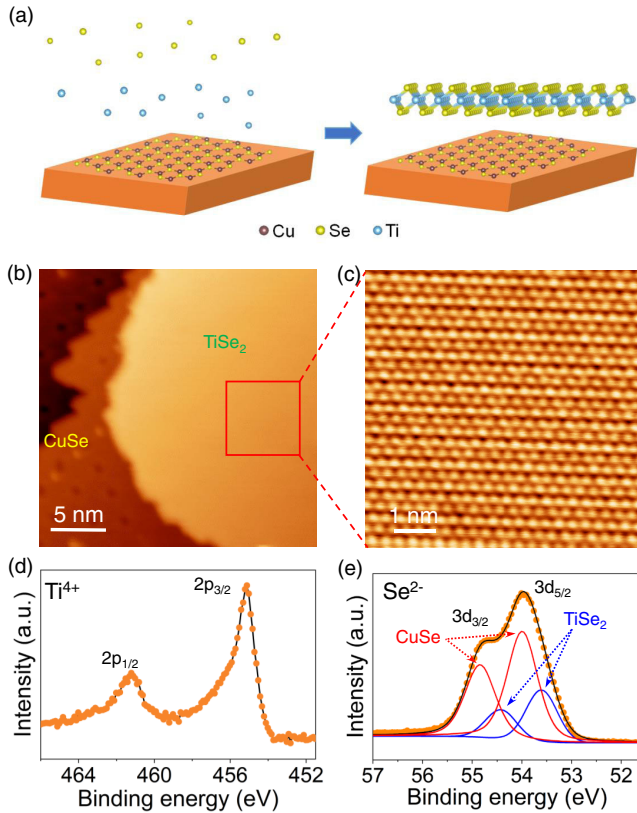


FIG. 1. (a) Schematic illustrations of the growth process and the structure of monolayer  $\text{TiSe}_2/\text{CuSe}/\text{Cu}(111)$ . (b) Large-scale STM image of monolayer  $\text{TiSe}_2$  grown on  $\text{CuSe}/\text{Cu}(111)$  ( $V_S = -2$  V,  $I_S = 50$  pA,  $T = 80$  K). (c) High-resolution STM image of monolayer  $M\text{-TiSe}_2$  in the red square in (b) ( $V_S = -50$  mV,  $I_S = 1$  nA,  $T = 80$  K). (d) XPS of the  $\text{Ti } 2p$  core levels. (e) XPS of the  $\text{Se } 3d$  core levels. The blue and red curves are fitting curves corresponding to the  $\text{Se } 3d$  core levels from  $\text{TiSe}_2$  and  $\text{CuSe}$ , respectively. Discrete points represent the raw data and the black line is the fitting line.

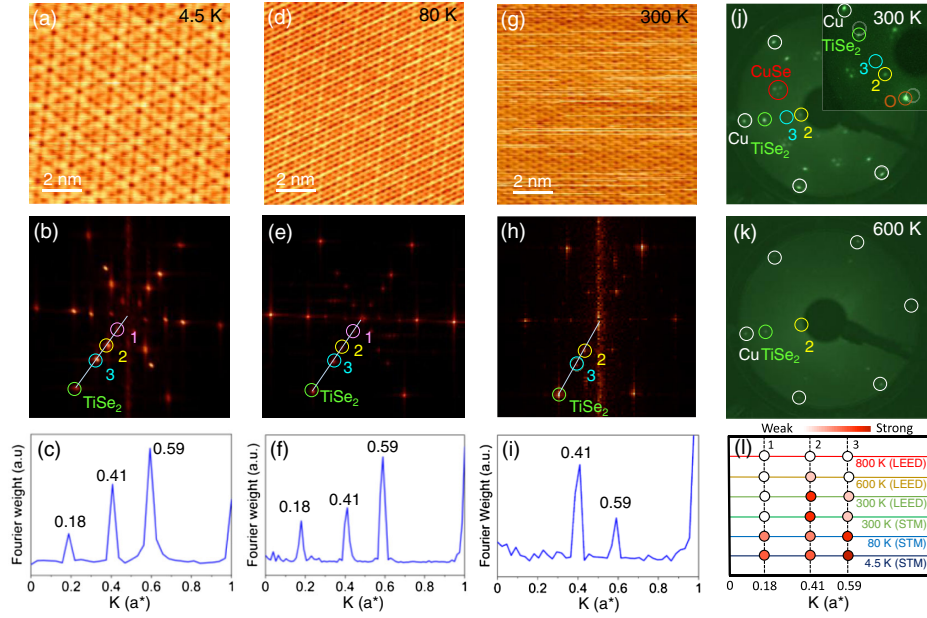


FIG. 2. (a),(d), and (g) High-resolution STM images of monolayer-TiSe<sub>2</sub>/CuSe/Cu(111) at different temperatures, showing the superstructure. The scanning parameters are  $V_S = -0.05$  V,  $I_S = 0.1$  nA in (a), and  $V_S = -1$  V,  $I_S = 1$  nA in (d) and (g), respectively. (b),(e), and (h) Fast Fourier transform (FFT) of STM images in (a),(d), and (g), respectively. The circles indicate the positions of the superstructure. (c),(f), and (i) Representative line cuts from the central point to TiSe<sub>2</sub> point in (b),(e), and (h), respectively. (j) LEED pattern of the sample at 300 K, showing diffraction spots from Cu(111) substrate (white circles), TiSe<sub>2</sub> (green circle), CuSe (red circle), two superstructure peaks 2 and 3 (yellow and cyan circles). The inset is the same LEED pattern with the sample rotated, so that the central area close to the reflected spot of incident electron beam (brown circle) is visible, showing the absence of peak 1 at this temperature. (k) LEED pattern of the sample at 600 K, showing one superstructure peak 2. (l) Schematic drawing of variations of the superstructure peaks with temperature.

with the room temperature LEED pattern in Fig. 2(j). The sample is also tilted by an angle so that the diffraction space close to the central area is visible [inset, Fig. 2(j)]. By doing this check, we verified the disappearance of peak 1 in LEED pattern. The six diffraction spots highlighted by the white circles originate from the sixfold symmetry of the Cu(111) substrate and the diffraction spots (marked by the red circles) are assigned to the CuSe lattice and patterned nanopores in CuSe layer [29]. The six diffraction spots (marked by the green circle) are assigned to the *M*-TiSe<sub>2</sub> lattice and the two sets of spots (marked by yellow and cyan circles) are due to the superstructure of TiSe<sub>2</sub> at room temperature.

In order to exclude the possibility that the superstructure is moiré superlattices, we calculated the possible moiré periodicity of the TiSe<sub>2</sub>/CuSe structure by substituting the lattice period of TiSe<sub>2</sub> ( $\sim 3.37$  Å) and CuSe ( $\sim 4.06$  Å) and the rotation angle ( $30^\circ$ ) into the formula of moiré-pattern periodicity [32,33]. The calculated periodicity of the moiré superstructure is  $\sim 6.72$  Å ( $\sim 0.50 \times a^*$ ), which is not what we observe in the experiments. This result suggests that what we observed in STM images does not originate from the moiré superstructure between CuSe and TiSe<sub>2</sub>.

At low temperature, peak 3 is the brightest in FFT of STM images, indicating that  $q = 0.59a^*$  is the main wave vector, and  $0.18a^*$  (peak 1) =  $2q - 1$ ,  $0.41a^*$

(peak 2) =  $1 - q$  are different orders of the main wave vector. The relationship of these superstructure wave vectors is similar to that of TbTe<sub>3</sub> [34], whose superstructure is interpreted as incommensurate CDW (I-CDW). In order to describe the evolution of the superstructure with temperature more clearly, we plot the superstructure peaks' positions of TiSe<sub>2</sub>/CuSe/Cu(111) obtained under different temperatures in Fig. 2(l). We find that the number of superstructure peaks decreases as the temperature rises. The main wave vector changes from the position of peak 3 at low temperature to the position of peak 2 at high temperature. Further increase of the temperature results in a LEED pattern with only peak 2 at about 600 K [Fig. 2(k)] and without any features above 800 K, which indicates that a phase transition occurs at a temperature higher than 600 K in monolayer TiSe<sub>2</sub>/CuSe heterostructure. Both the correlation of these wave vectors and the phase transition at high temperature corroborate that the superstructure we observed is an I-CDW.

Compared with TaS<sub>2</sub>, which shows an I-CDW phase ranging from 350 to 550 K and undergoes near commensurate CDW (NC-CDW) and commensurate CDW (C-CDW) transition at low temperatures [35], *M*-TiSe<sub>2</sub> exhibits a single I-CDW phase below 600 K. The fractional CDW wave factors in *M*-TiSe<sub>2</sub> are different from previous reports on incommensurate CDW in TiSe<sub>2</sub>, in which the

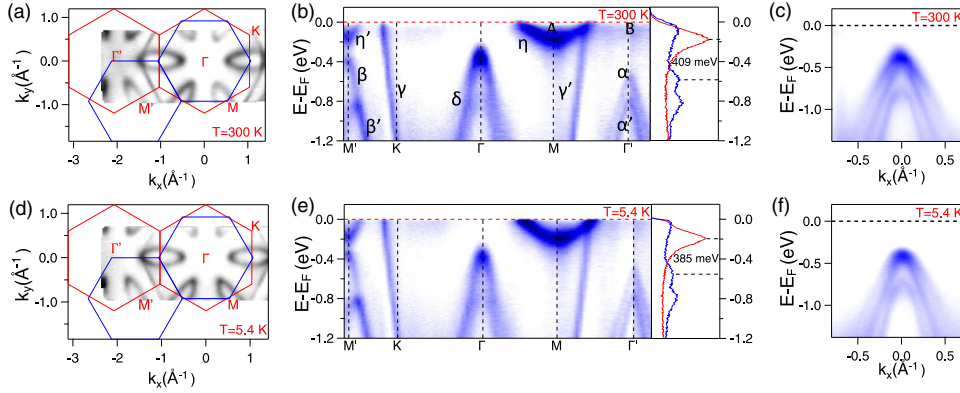


FIG. 3. (a) and (d) Constant-energy map at  $E_F$ , obtained by ARPES, at 300 and 5.4 K, respectively. The Brillouin zones of  $\text{TiSe}_2$  and  $\text{CuSe}$  are indicated by the red and blue hexagons. (b) and (e) ARPES intensity plots along  $M' - \Gamma - \Gamma'$  at 300 and 5.4 K, respectively. The red and blue curves are energy distribution curves (EDCs) at  $M$  and  $\Gamma'$ . (c) and (f) Detailed electronic band around  $\Gamma$  (along  $\Gamma - M$  direction) at 300 and 5.4 K, respectively.

incommensuration is caused by domain walls and the CDW wave vector only changes slightly from commensuration [7,26].

In order to study the electronic structure of the monolayer- $\text{TiSe}_2/\text{CuSe}$  heterostructure, we characterized the sample using ARPES at low and room temperatures. The photoemission intensity maps at Fermi level ( $E_F$ ) measured at room temperature and 5.4 K are shown in Figs. 3(a) and 3(d), respectively. These two full-scale maps show hexagonal symmetry, which is consistent with the symmetry of the  $\text{TiSe}_2/\text{CuSe}/\text{Cu}(111)$  sample. The clear elliptical Fermi pocket around the  $M$  point is similar to that of  $(\text{PbSe})_{1.16}(\text{TiSe}_2)_m$  ( $m = 1, 2$ ) heterostructure [36], but the  $M$ - $\text{TiSe}_2$  here has much heavier electron doping at both 5.4 and 300 K. The electron doping level could be figured out by counting Luttinger volumes of the Fermi pockets [36,37], which gives a doping level of  $0.6e^-$  per  $\text{TiSe}_2$  at 5.4 K.

The momentum-resolved electronic structure of  $\text{TiSe}_2/\text{CuSe}/\text{Cu}(111)$  at 300 K is shown in Fig. 3(b), which presents the ARPES intensity plots measured along the  $\Gamma - M - \Gamma'$  and  $\Gamma - K - M'$ . In order to differentiate the band structures of Se in  $\text{TiSe}_2$  and  $\text{CuSe}$ , the second Brillouin zone was mapped. The  $\Gamma'$  point is the center of the second Brillouin zone of  $M$ - $\text{TiSe}_2$ , and the band structures ( $\alpha$  and  $\alpha'$ ) around  $\Gamma'$  should be the same as the  $\Gamma$  point of  $\text{TiSe}_2$  because of translational symmetry. The curved bands of  $\eta$  and  $\eta'$  come from  $\text{Ti } 3d$  bands, while  $\alpha$  and  $\alpha'$  are associated with spin-orbit split of  $\text{Se } 4p$  bands. They are similar with those of bulk  $\text{TiSe}_2$  [4], except that the bands in our sample are shifted vertically. The two bands  $\beta$  and  $\beta'$  in the second Brillouin zone come from Se in monolayer  $\text{CuSe}$ . Two electronlike bands ( $\gamma$  and  $\gamma'$ ) are attributed to  $\text{Cu}(111)$ , consistent with previous ARPES measurements [38]. Obviously, the  $\delta$  bands around the  $\Gamma$  point are simple superposition of  $\alpha$ ,  $\alpha'$ ,  $\beta$ , and  $\beta'$ .

Pristine  $\text{TiSe}_2$  opens a small indirect band gap near the Fermi level when undergoing a commensurate ( $2 \times 2 \times 2$ )

CDW transition at  $T_{\text{CDW}} \approx 200$  K [4,39,40], and the experiments and calculations of  $\text{Cu}$ -intercalated  $\text{TiSe}_2$  indicate a gap opening below the Fermi level and its shifting to lower energies with increasing  $\text{Cu}$  content [1,25]. The position of the energy gap in the monolayer  $\text{TiSe}_2/\text{CuSe}$  heterostructure in this work is similar to that of the  $\text{Cu}$ -intercalated bulk  $\text{TiSe}_2$ . We can see that a large indirect gap opened below the Fermi level at room temperature ( $T = 300$  K). The band gap is about 409 meV, which is derived from the energy distribution curves [right panel of Fig. 3(b)] including the red curve along  $A - M$  and the blue curve along  $B - \Gamma'$  in the left panel of Fig. 3(b). In particular, for the incommensurate structure, the Brillouin zone will not shrink by an integral multiple to form a complete period and the electronic state will not be folded, so no folding bands in ARPES have been observed. Combining the superstructure observed by STM and LEED, we conclude that I-CDW appears at room temperature. In Figs. 3(c) and 3(f), we present detailed electronic bands around  $\Gamma$ . In Fig. 3(e), the electronic bands taken at low temperature ( $T = 5.4$  K) exhibit a smaller gap (385 meV) compared with that at room temperature.

On the basis of these experimental data, we discuss the possible mechanism of the existence of the I-CDW in  $M$ - $\text{TiSe}_2$ . The measured band structures of  $M$ - $\text{TiSe}_2$  show that the existence of the  $\text{CuSe}/\text{Cu}(111)$  substrate moves the Fermi level of  $\text{TiSe}_2$  deeper into the conduction band compared to the pristine  $\text{TiSe}_2$ , so we rule out the possibility of Fermi surface nesting as the mechanism. The excitonic condensate mechanism is based on a semimetal with a small band gap near the Fermi level. This mechanism does not apply in this case, because the electron-hole direct Coulomb interaction is screened out by a mass of charge carriers in the semimetal. The Jahn-Teller effect, a possible mechanism to explain CDW in pristine  $\text{TiSe}_2$ , is based on that the  $\text{Se } 4p$  valence band and the  $\text{Ti } 3d$  conduction band are lowered to open a bigger gap upon cooling [13]. From our ARPES data, we can see that

both the Se  $4p$  valance band at  $\Gamma'$  and the Ti  $3d$  conduction band at  $M$  are lowered at 300 and 5.4 K compared to pristine  $\text{TiSe}_2$ , and the electron bands taken at low temperature ( $T = 5.4$  K) exhibit a smaller indirect gap below the Fermi level compared to that at room temperature ( $T = 300$  K). Thus, the Jahn-Teller mechanism cannot be used to explain the I-CDW in  $M$ - $\text{TiSe}_2$  either. The superstructure in  $M$ - $\text{TiSe}_2$  is very unique compared to previous reports, including the commensurate ( $2 \times 2 \times 2$ ) superstructure in bulk  $\text{TiSe}_2$  below 200 K [3] and the incommensurate superstructure in Cu-intercalated bulk 1T- $\text{TiSe}_2$  at low temperature [26]. Obviously, monolayer  $\text{CuSe}/\text{Cu}(111)$  substrates are the key factor for the formation of the I-CDW phase. Therefore, we would suggest that the mechanism of the origin of the I-CDW in  $M$ - $\text{TiSe}_2$  is associated with the interface effect. Previous reports support this possible mechanism. For example, CDW occurs when monolayer  $\text{TiTe}_2$  is grown on top of monolayer  $\text{PtTe}_2$ , but no CDW transitions are seen in  $N$ -layer  $\text{PtTe}_2$  ( $N = 2, 3$ , and 4), which indicate the modulation of CDW by interface effect between monolayers [41]. In another experiment, when  $\text{TiTe}_2$  is grown on a graphene-terminated SiC surface, monolayer  $\text{TiTe}_2$  exhibits CDW transition below 92 K, but the CDW is suppressed in thicker films even with just two layers [42]. This experimental example again shows that CDW is modulated by interface effect.

In summary, by using a three-step epitaxial method, we fabricated a monolayer  $\text{TiSe}_2/\text{CuSe}$  heterostructure on a  $\text{Cu}(111)$  substrate. In this heterostructure, we observed a new type of phase of the I-CDW. Remarkably,  $M$ - $\text{TiSe}_2$  displays an I-CDW phase below 600 K with strong electron doping. We suggest that the mechanism for I-CDW formation in the  $M$ - $\text{TiSe}_2$  may be the interface effect. The results provide a new platform to study the CDW in two-dimensional materials.

We thank Sokrates T. Pantelides, Min Ouyang, and Wei Ji for fruitful discussions. We acknowledge financial support from the National Key R&D Program of China (Grants No. 2018YFA0305800 and No. 2019YFA0308500), the National Natural Science Foundation of China (Grants No. 61925111, No. 61725107, No. 61888102, and No. 51572290), the Strategic Priority Research Program of Chinese Academy of Sciences (Grants No. XDB28000000 and No. XDB30000000), CAS Project for Young Scientists in Basic Research (YSBR-003), the Fundamental Research Funds for the Central Universities and the CAS Key Laboratory of Vacuum Physics.

\*Corresponding author.  
luhl@ucas.ac.cn

†Corresponding author.  
xlin@ucas.ac.cn

[1] X. Zhu, J. Guo, J. Zhang, and E. W. Plummer, *Adv. Phys.* **2**, 622 (2017).

- [2] B. Singh, C.-H. Hsu, W.-F. Tsai, V. M. Pereira, and H. Lin, *Phys. Rev. B* **95**, 245136 (2017).
- [3] F. J. Disalvo, D. E. Moncton, and J. V. Waszczak, *Phys. Rev. B* **14**, 4321 (1976).
- [4] T. E. Kidd, T. Miller, M. Y. Chou, and T. C. Chiang, *Phys. Rev. Lett.* **88**, 226402 (2002).
- [5] G. Li, W. Z. Hu, D. Qian, D. Hsieh, M. Z. Hasan, E. Morosan, R. J. Cava, and N. L. Wang, *Phys. Rev. Lett.* **99**, 027404 (2007).
- [6] B. Hildebrand, C. Didiot, A. M. Novello, G. Monney, A. Scarfato, A. Ubaldini, H. Berger, D. R. Bowler, C. Renner, and P. Aebi, *Phys. Rev. Lett.* **112**, 197001 (2014).
- [7] Y. I. Joe, X. M. Chen, P. Ghaemi, K. D. Finkelstein, G. A. de la Peña, Y. Gan, J. C. T. Lee, S. Yuan, J. Geck, G. J. MacDougall, T. C. Chiang, S. L. Cooper, E. Fradkin, and P. Abbamonte, *Nat. Phys.* **10**, 421 (2014).
- [8] B. Singh, C. H. Hsu, W. F. Tsai, V. M. Pereira, and H. Lin, *Phys. Rev. B* **95**, 245136 (2017).
- [9] B. Hildebrand, T. Jaouen, M. L. Mottas, G. Monney, C. Barreateau, E. Giannini, D. R. Bowler, and P. Aebi, *Phys. Rev. Lett.* **120**, 136404 (2018).
- [10] A. Zunger and A. J. Freeman, *Phys. Rev. B* **17**, 1839 (1978).
- [11] K. Rossnagel, *J. Phys. Condens. Matter* **23**, 213001 (2011).
- [12] H. P. Hughes, *J. Phys. C* **10**, L319 (1977).
- [13] K. Rossnagel, L. Kipp, and M. Skibowski, *Phys. Rev. B* **65**, 235101 (2002).
- [14] M. Calandra and F. Mauri, *Phys. Rev. Lett.* **106**, 196406 (2011).
- [15] F. Weber, S. Rosenkranz, J. P. Castellán, R. Osborn, G. Karapetrov, R. Hott, R. Heid, K. P. Bohnen, and A. Alatas, *Phys. Rev. Lett.* **107**, 266401 (2011).
- [16] D. Jerome, T. M. Rice, and W. Kohn, *Phys. Rev.* **158**, 462 (1967).
- [17] W. Kohn, *Phys. Rev. Lett.* **19**, 439 (1967).
- [18] C. S. Snow, J. F. Karpus, S. L. Cooper, T. E. Kidd, and T. C. Chiang, *Phys. Rev. Lett.* **91**, 136402 (2003).
- [19] C. Monney, H. Cercellier, F. Clerc, C. Battaglia, E. F. Schwier, C. Didiot, M. G. Garnier, H. Beck, P. Aebi, H. Berger, L. Forró, and L. Patthey, *Phys. Rev. B* **79**, 045116 (2009).
- [20] M. M. May, C. Brabetz, C. Janowitz, and R. Manzke, *Phys. Rev. Lett.* **107**, 176405 (2011).
- [21] E. Moehr-Vorobeva, S. L. Johnson, P. Beaud, U. Staub, R. De Souza, C. Milne, G. Ingold, J. Demsar, H. Schaefer, and A. Titov, *Phys. Rev. Lett.* **107**, 036403 (2011).
- [22] C. Monney, C. Battaglia, H. Cercellier, P. Aebi, and H. Beck, *Phys. Rev. Lett.* **106**, 106404 (2011).
- [23] G. Monney, C. Monney, B. Hildebrand, P. Aebi, and H. Beck, *Phys. Rev. Lett.* **114**, 086402 (2015).
- [24] E. Morosan, H. W. Zandbergen, B. S. Dennis, J. W. G. Bos, Y. Onose, T. Klimczuk, A. P. Ramirez, N. P. Ong, and R. J. Cava, *Nat. Phys.* **2**, 544 (2006).
- [25] A. M. Novello, M. Spera, A. Scarfato, A. Ubaldini, E. Giannini, D. R. Bowler, and C. Renner, *Phys. Rev. Lett.* **118**, 017002 (2017).
- [26] S. Yan, D. Iaia, E. Morosan, E. Fradkin, P. Abbamonte, and V. Madhavan, *Phys. Rev. Lett.* **118**, 106405 (2017).
- [27] B. Hildebrand, T. Jaouen, C. Didiot, E. Razzoli, G. Monney, M.-L. Mottas, A. Ubaldini, H. Berger, C. Barreateau, H. Beck, D. R. Bowler, and P. Aebi, *Phys. Rev. B* **93**, 125140 (2016).

- [28] L. J. Li, E. C. T. O'Farrell, K. P. Loh, G. Eda, B. Ozyilmaz, and A. H. C. Neto, *Nature (London)* **529**, 185 (2016).
- [29] X. Lin *et al.* *Nat. Mater.* **16**, 717 (2017).
- [30] J. P. Peng, J. Q. Guan, H. M. Zhang, C. L. Song, L. L. Wang, K. He, Q. K. Xue, and X. C. Ma, *Phys. Rev. B* **91**, 121113 (2015).
- [31] A. S. Shkvarin, Y. M. Yarmoshenko, M. V. Yablonskikh, A. I. Merentsov, E. G. Shkvarina, A. A. Titov, Y. M. Zhukov, and A. N. Titov, *J. Chem. Phys.* **144**, 074702 (2016).
- [32] G. Oster, C. Zwerling, and M. Wasserman, *J. Opt. Soc. Am.* **54**, 169 (1964).
- [33] J. Martinez-Castro, D. Mauro, A. Pasztor, I. Gutierrez-Lezama, A. Scarfato, A. F. Morpurgo, and C. Renner, *Nano Lett.* **18**, 6696 (2018).
- [34] A. Fang, N. Ru, I. R. Fisher, and A. Kapitulnik, *Phys. Rev. Lett.* **99**, 046401 (2007).
- [35] B. Sipos, A. F. Kusmartseva, A. Akrap, H. Berger, L. Forro, and E. Tutis, *Nat. Mater.* **7**, 960 (2008).
- [36] Q. Yao, D. W. Shen, C. H. P. Wen, C. Q. Hua, L. Q. Zhang, N. Z. Wang, X. H. Niu, Q. Y. Chen, P. Dudin, Y. H. Lu, Y. Zheng, X. H. Chen, X. G. Wan, and D. L. Feng, *Phys. Rev. Lett.* **120**, 106401 (2018).
- [37] J. M. Luttinger and J. C. Ward, *Phys. Rev.* **118**, 1417 (1960).
- [38] L. Gao, J.-T. Sun, J.-C. Lu, H. Li, K. Qian, S. Zhang, Y.-Y. Zhang, T. Qian, H. Ding, X. Lin, S. X. Du, and H.-J. Gao, *Adv. Mater.* **30**, 1707055 (2018).
- [39] H. Cercellier, C. Monney, F. Clerc, C. Battaglia, L. Despont, M. G. Garnier, H. Beck, P. Aebi, L. Patthey, H. Berger, and L. Forró, *Phys. Rev. Lett.* **99**, 146403 (2007).
- [40] J. C. E. Rasch, T. Stemmler, B. Mueller, L. Dudy, and R. Manzke, *Phys. Rev. Lett.* **101**, 237602 (2008).
- [41] M.-K. Lin, J. A. Hlevyack, P. Chen, R.-Y. Liu, S.-K. Mo, and T. C. Chiang, *Phys. Rev. Lett.* **125**, 176405 (2020).
- [42] P. Chen, W. W. Pai, Y.-H. Chan, A. Takayama, C.-Z. Xu, A. Karn, S. Hasegawa, M. Y. Chou, S.-K. Mo, A.-V. Fedorov, and T.-C. Chiang, *Nat. Commun.* **8**, 516 (2017).